Journal Name

ARTICLE TYPE

Cite this: DOI: 10.1039/xxxxxxxxxx

Engineering New Defective Phases of UiO Family Metal-Organic Frameworks with Water†

Francesca C.N. Firth,[a] Matthew J. Cliffe,‡[a] Diana Vulpe,[b] Marta Aragones-Anglada,[b] Peyman Z. Moghadam,[c] David Fairen-Jimenez,[b] Ben Slater[d] and Clare P. Grey*[a]

Received Date
Accepted Date

DOI: 10.1039/xxxxxxxxxx

www.rsc.org/journalname

As defects significantly affect the properties of metal-organic frameworks (MOFs)–from changing their mechanical properties to enhancing their catalytic ability–obtaining synthetic control over defects is essential to tuning the effects on the properties of the MOF. Previous work has shown that synthesis temperature and the identity and concentration of modulating acid are critical factors in determining the nature and distribution of defects in the UiO family of MOFs. In this paper we demonstrate that the amount of water in the reaction mixture in the synthesis of UiO family MOFs is an equally important factor, as it controls the phase which forms for both UiO-67(Hf) and UiO-66(Hf) (F_4BDC). We use this new understanding of the importance of water to develop a new route to the stable defect-ordered **hcp** UiO-66(Hf) phase, demonstrating the effectiveness of this method of defect-engineering in the rational design of MOFs. The insights provided by this investigation open up the possibility of harnessing defects to produce new phases and dimensionalities of other MOFs, including nanosheets, for a variety of applications such as MOF-based membranes.

1 Introduction

The UiO family of MOFs is of great interest for real-world applications, including sensing and energy storage.[1–5] UiO-66 (the prototypical UiO framework) is particularly thermally and chemically stable,[6,7] due to the high coordination of its hexanuclear $M_6(\mu_3\text{-O})_4(\mu_3\text{-OH})_4$ metal clusters (M = Hf, Zr) by 12 linear dicarboxylate linkers in a face-centred cubic topology.[8,9] As well as stability, this family of MOFs possesses catalytic activity and gas sorption capabilities,[10,11] and the use of organic linkers with different functionalities can give access to new or improved properties such as increased CO_2 adsorption.[12,13]

Zirconium and hafnium MOFs, including the UiO family, exhibit a wide range of defect chemistry. As defects alter the properties of the framework, obtaining control over the type, location and concentration of defects will in turn allow control over the properties of the MOF.[9,14–17] UiO-66 is an ideal system for studying defective MOFs,[18] as it commonly incorporates both linker and cluster vacancies.[15,19] The framework remains stable despite the presence of these defects due to the strong metal-linker coordination and high connectivity of the framework.[20]

Missing-linker defects require compensating 'capping' ligands at coordination sites on the metal cluster left vacant by the absence of linkers; these capping ligands are usually derived from other species (such as solvent or counterions) present during the synthesis.[9,21,22] Defects can therefore be deliberately introduced via the inclusion of these species in the reaction mixture.[23–28] In 'modulated' synthesis, a monocarboxlic acid modulator is included in the synthesis, giving a ready source of monocarboxylate groups that compete with the linker to coordinate to the cluster, thereby creating missing-linker defects.[1,14,21,29] While modulated synthesis was originally devised as a method of controlling the morphology of MOF crystals via capping coordination sites on the faces of the MOF crystal,[30–32] the linker vacancies introduced by modulated synthesis can be incorporated within the framework, leading to a defective structure. By altering the identity and concentration of the modulator included in the synthesis, the concentration of linker vacancies in a MOF can be tuned systematically.[1,14,33]

In our previous work, we showed that the use of modulating formic acid enabled control over the spatial distribution of defects in UiO family MOFs.[9,19] In UiO-66(Hf), correlation of missing-linker defects around the clusters, compensated by the modu-

[a] Department of Chemistry, University of Cambridge CB2 1EW, UK. E-mail: cpg27@cam.ac.uk
[b] Department of Chemical Engineering and Biotechnology, University of Cambridge CB3 0AS, UK
[c] Department of Chemical and Biological Engineering, University of Sheffield S1 3JD, UK
[d] Department of Chemistry, University College London WC1H OAJ, UK
† Electronic Supplementary Information (ESI) available: additional PXRD data, solution NMR, TGA data and models. See DOI: 10.1039/b000000x/
‡ 'Present address:' School of Chemistry, University of Nottingham NG7 2RD, UK.

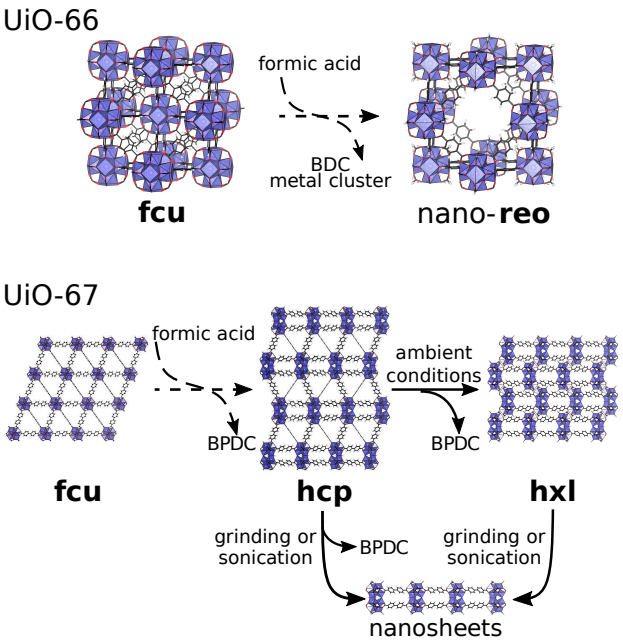

Fig. 1 Reported phases of UiO-66 (top; formed with terephthalate ('BDC') linkers) and UiO-67 (bottom; formed with biphenyldicarboxylate ('BPDC') linkers). Dashed arrows show the differences in the synthesis conditions required in order to obtain different phases; solid arrows show postsynthetic treatments. Structural models derived from crystallographic information files reported in Refs. 6,9,19.

lator, leads to the introduction of cluster vacancies correlated along ⟨100⟩ directions in the **fcu** matrix, forming correlated nano-domains with the **reo** (primitive cubic) topology [Fig. 1].[19,21] In UiO-66(Hf), complete defect ordering is prevented by the concomitant formation of a $Hf_6O_4(OH)_4(FcO)_{12}$ hafnium formate layered framework as modulator concentration increases.[19,34]

However, using modulating formic acid in the synthesis of UiO-67(Hf) results in the formation of a new defect-ordered phase.[9] In this UiO-67(Hf) phase, the missing-linker defects order within a (111) plane of the parent **fcu** structure, resulting in the condensation of pairs of 12-coordinate $M_6(\mu_3\text{-O})_4(\mu_3\text{-OH})_4$ clusters into 18-coordinate $[M_6(\mu_3\text{-O})_4(\mu_3\text{-OH})_4]_2(\mu_2\text{-OH})_6$ double clusters, giving a hexagonal **hcp** topology [Fig. 1].[9] The structural relationship between the **fcu** and **hcp** frameworks can be visualised by distorting the cubic structure along the [111] direction, so that the (111) plane of the **fcu** structure corresponds to the (001) plane of the **hcp**. This relationship means that the powder X-ray diffraction patterns are also closely related, as the **fcu** (111) reflection, corresponding to the close-packed plane, is replaced by reflections corresponding to the (002), (100) and (101) pseudo-close-packed planes in the **hcp** structure. Therefore, these two phases can be differentiated by the presence of these reflections. Rather than nano-domains, **hcp** UiO-67(Hf) is obtained as an ordered single phase bulk material.

These new defective frameworks have different properties from the parent non-defective UiO frameworks. Nano **reo** UiO-66(Hf) displays significantly enhanced high-pressure gravimetric gas sorption compared to **fcu** UiO-66(Hf).[11] In **hcp** UiO-67(Hf), the directionality of the structure means that selective topotactic delamination under gentle conditions produces the crystalline layered **hxl** structure, and under more forcing conditions (such as sonication or grinding) gives two-dimensional nanosheets, hereafter named **hns** UiO-67(Hf) [Fig. 1].[9,11,35]

While defect engineering is becoming increasingly recognised as an important technique for tuning the properties of frameworks,[11,36,37] the factors determining control over the degree and correlation of defects are not well understood. In contrast to the use of modulated synthesis,[14,38] the influence of water in the reaction mixture on the formation of defect phases of UiO family MOFs is not well-explored. This is despite water being essential for the formation of the metal cluster in UiO family MOFs, and in a wider chemical context, playing a critical role in zirconium and hafnium solution chemistry.[23,25,39–41] Additionally, while hydrothermal syntheses of UiO family MOFs are particularly environmentally attractive, as they remove the need to use toxic organic solvents such as DMF, there has been little specific investigation into the potential effects on the phase of the MOF framework of using water as a solvent. Previously reported syntheses of UiO-66 (F_4BDC) (UiO-66 with tetrafluoroterephthalate linkers) with and without water produce diffraction patterns indicative of different phases, but this has until now not been explained.[42–44] Additionally, although the **hcp** topology has been reported for UiO MOFs formed from other ligands, such as 2,2'-bipyridinedicarboxylate and (nitro)triphenyldicarboxylate[45] since our synthesis of **hcp** UiO-67(Hf), the archetypal **hcp** UiO-66 material was until recently unknown, and has only been synthesised using ionic liquids rather than a more standard solvothermal synthesis.[46]

In this work we systematically investigate the role of water in the formation of defect phases of UiO family MOFs, using a combination of synthesis, powder X-ray diffraction, thermogravimetric analysis and quantum chemical calculations. By varying the amount of water in the synthesis we demonstrate that, alongside formic acid, water is crucial to the successful synthesis of **hcp** UiO-67(Hf) and, additionally, that water allows the direct synthesis of the layered-nanosheet phase **hns** UiO-67(Hf). We use this knowledge to explain both reported and new phases of UiO-66(Hf) (F_4BDC) and then to synthesise **hcp** UiO-66(Hf) using conventional solvents. All UiO MOFs synthesised for this report are the hafnium analogues, unless otherwise specified.

2 Experimental

2.1 Synthesis

All reagents used were obtained from commercial suppliers and used without further purification.

2.1.1 Synthesis of UiO-67(Hf) defect phases.

Procedure modified from Ref. 9. $HfCl_4$ (Acros Organics, 99 %, 0.3 mmol, 96.1 mg) and biphenyldicarboxylic acid (H_2BPDC) (Acros Organics, 98 %, 0.3 mmol, 72.6 mg) were added to a 23 mL PTFE-lined steel autoclave, followed by dry *N,N*-dimethylformamide (DMF) (Sigma Aldrich, 99.85 % anhydrous DMF) (4 mL), and varying amounts of formic acid (Fisher, 98/100 %) (0.25–2 mL) and water (0–0.2 mL). The autoclave

was sealed and heated at 150°C for 24 hours. The resulting white microcrystalline powder was filtered under vacuum, washed on the filter (DMF, Alfa Aesar, 99 %, 5 mL) and the solid product dried. Phase-pure **hcp** UiO-67 formed with 1 mL formic acid and 0.05 mL water. Phase-pure **hns** UiO-67 formed with 1 mL formic acid and 0.2 mL water.

2.1.2 Synthesis of UiO-66(Hf) defect phases.

$HfCl_4$ (Acros Organics, 99 %, 0.3 mmol, 96.1 mg) and terephthalic acid (H_2BDC) (Alfa Aesar, 98 %, 0.3 mmol, 49.8 mg) were added to a 23 mL PTFE-lined steel autoclave, followed by dry *N,N*-dimethylformamide (Sigma Aldrich, 99.85 % anhydrous DMF) (4 mL), and varying amounts of formic acid (Fisher, 98/100 %) (0.5–3.0 mL) and water (0–3.5 mL). The autoclave was sealed and heated at 150°C for 24 hours. The resulting white microcrystalline powder was filtered under vacuum, washed on the filter (DMF, Alfa Aesar, 99 %, 5 mL) and the solid product dried. Phase-pure **hcp** UiO-66 formed with 1.5 mL formic acid and 0.4 mL water.

2.1.3 Hydrothermal synthesis of UiO-66(Hf) (F_4BDC) phases.

Procedure adapted from Ref. 43. $HfCl_4$ (Acros Organics, 99 %, 0.1 mmol, 32.0 mg) and tetrafluoroterephthalic acid (H_2F_4BDC) (Sigma, 97 %, 0.1 mmol, 23.8 mg) were added to a 23 mL PTFE-lined steel autoclave, followed by varying ratios of water and acetic acid (Sigma-Aldrich, >99.7 %) (0.96 mL solvent in ratios from 0:100 to 100:0 water:acid v/v). The autoclave was sealed and heated at 120°C or 150°C for 24 hours. The resulting white microcrystalline powder was filtered under vacuum, washed on the filter (water, 5 mL) and the solid product dried. Phase-pure **hcp** UiO-66(Hf) (F_4BDC) was synthesised at 120°C, with 60:40 water:acetic acid. This synthesis was further scaled up to $HfCl_4$ (0.3 mmol, 96.1 mg), H_2F_4BDC (0.3 mmol, 71.4 mg), water (1.73 mL) and acetic acid (1.15 mL). The **hcp** zirconium analogue was synthesised under the same conditions but with $ZrCl_4$ as the source of metal ions. The **hcp** structure was also produced when the modulating acetic acid was replaced with the same volume of formic acid.

2.1.4 Anhydrous synthesis of fcu UiO-66(Hf) (F_4BDC).

Procedure adapted from Ref. 44. $HfCl_4$ ((Acros Organics, 99 %, 0.1 mmol, 32.0 mg) and tetrafluoroterephthalic acid (H_2F_4BDC) (Sigma, 97 %, 0.1 mmol, 23.8 mg) were added to a 23 mL PTFE-lined steel autoclave, followed by tetrahydrofuran (THF) (Fisher, analytical grade, 4 mL) and hydrochloric acid (Honeywell Fluka, fuming, 36.5-38 %, 42 μL). The autoclave was sealed and heated at 80°C for 24 hours. The resulting white microcrystalline powder was filtered under vacuum, washed on the filter (THF, Fisher, analytical grade, 5 mL) and the solid product dried.

2.2 Characterisation

2.2.1 Sample washing and activation method.

Procedure adapted from Ref. 14. Unreacted ligand was removed from the sample by washing with DMF at 70°C for 24 hours, followed by two further 2-hour washing cycles. After each wash, residual DMF was removed after centrifugation of the mixture at 8000 rpm for 15 minutes. Finally, any residual DMF was removed by heating at 200°C for 24 hours.

2.2.2 Powder X-ray diffraction.

The crystal structure, purity and crystallinity for all samples were assessed via their powder X-ray diffraction (PXRD) patterns, measured using a PANalytical Empyrean diffractometer (Cu Kα radiation, λ = 1.541 Å) over the 2θ range 3-40°, using a step size of 0.017° and a scan speed of 0.13°s^{-1}. Longer scans on some samples were performed with a step size of 0.017° and scan speed of 0.022°s^{-1}. Analysis of all powder diffraction data was carried out using the TOPAS Academic 4.1 structure refinement software.[47–49] Simulated powder patterns of different MOF phases were obtained using Mercury and Vesta software.[50,51]

2.2.3 Solution NMR.

Solution NMR was used to probe the nature of the organic components of the samples. The samples were prepared using a method adapted from Ref. 14. 10 mg of sample, washed and activated as described above, was digested in 1 M NaOH (Breckland Scientific Supplies Ltd.) in D_2O (Euro Isotop, 99 %, 600 μL). ^{1}H spectra of the resultant suspension [Figs. S12, S13†] were collected with a standard ^{1}H 500 MHz Bruker Avance AVIII HD Smart Probe.

2.2.4 Thermogravimetric Analysis.

Thermogravimetric analysis of samples was performed on a Mettler Toledo TGA/SDTA 851 thermo balance. Samples of 5–15 mg were heated to 700°C at a rate of 10°C min^{-1}. Measurements on samples were performed both under a constant flow (80 mL min^{-1}) of N_2 and under a constant flow (80 mL min^{-1}) of air (19-22 % O_2 in N_2), provided by Air Liquide UK Limited.

2.2.5 Scanning Electron Microscopy.

Samples were sputter coated with Pt to a thickness of 10 nm. Scanning electron microscopy was performed using a TESCAN MIRA3 FEG-SEM electron microscope operated at 5.0 kV, using the secondary electron detector.

2.2.6 Adsorption Measurements and Isotherms.

N_2 adsorption isotherms were carried out at 77 K on a Micromeritics 3Flex gas adsorption analyser. Samples were degassed in situ under vacuum at 120°C for 20 hours using the internal turbo pump. Warm and cold free-space correction measurements were performed using ultra-high purity He gas (grade 5.0, 99.999 % purity). Ultra-high purity N_2 (99.9992 %) was provided by Air products.

Grand canonical Monte Carlo (GCMC) simulations of N_2 adsorption were performed using the code RASPA.[53] During each GCMC cycle, translation, rotation, insertions, deletions, and regrow moves were attempted, using 10,000 equilibration cycles and 10,000 production cycles. Van der Waals interactions were described by 12-6 Lennard-Jones potential using a cut-off distance of 12.8 Å. The force field parameters for N_2 were taken from the TraPPE force field.[54] The Lennard-Jones parameters for the framework atoms were taken the Universal Force Field (UFF).[55] All MOFs were treated as rigid in the simulations. Adsorbate-

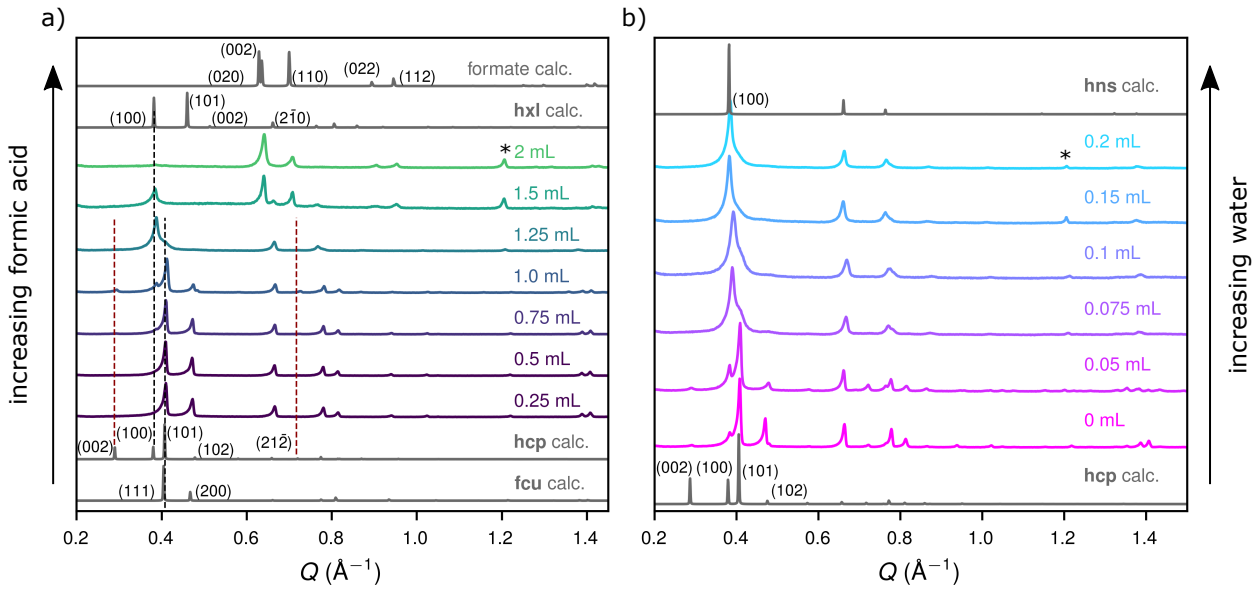

Fig. 2 a-b) PXRD patterns of UiO-67(Hf), synthesised with a) different concentrations of formic acid, b) with 1.0 mL of formic acid and different water concentrations, showing the dependency of the phase formed on the concentration of water. The calculated powder patterns of **fcu**,[52] **hcp**[9] and **hxl** UiO-67(Hf), and the hafnium formate MOF,[34] are shown for comparison. Dark red dashed lines indicate the evolution of peaks specific to the **hcp** phase, and black dashed lines show peaks which are common to more than one phase. Synthesis with 1.0 mL formic acid and 0.05 mL water gives phase-pure **hcp** UiO-67(Hf), and 0.2 mL water gives phase-pure **hns** UiO-67(Hf).

adsorbate and adsorbate-adsorbent van der Waals interactions were taken into account by Lorentz-Berthelot mixing rules.[56,57]

3 Results and discussion

3.1 The Role of Formic Acid and Water on UiO-67(Hf) Phases

Inspired by our previous work showing that formic acid plays a crucial role in the formation of the **hcp** UiO-67(Hf) phase,[9] we investigated the effect of different concentrations of formic acid in the synthesis of UiO-67(Hf) [Fig. 2(a)]. This series of syntheses was performed in DMF (99 %) but with no added water (i.e. we did not dry the as-received DMF).

Below 1 mL formic acid, the **fcu** phase is seen. **hcp** UiO-67(Hf) is formed when 1 mL formic acid (1:4 formic acid:DMF by volume) is used in the solvothermal synthesis: the observation of the **hcp**-characteristic peaks, (002), (100) and (101), in the region 0.28–0.41 Å^{-1} clearly indicate that the phase is different from **fcu**, which in this region only has a (111) reflection in the same position as the (101) reflection of **hcp**. As the volume of formic acid is increased above 1 mL, a new phase forms; at 1.5 mL FcOH this phase crystallises concomitantly alongside the known hafnium formate MOF. At around 2 mL formic acid only the formate MOF forms; at high concentrations of formic acid compared to that of BPDC, the formate anions outcompete in binding to the clusters.[21,34]

The powder X-ray diffraction (PXRD) pattern of the new material, seen most clearly in the PXRD patterns at 1.25 and 1.5 mL formic acid, strongly resembles that of the layered **hxl** UiO-67(Hf) material we previously reported,[9] but with absent *l*-dependent peaks, such as the (101) reflection, and with the remaining peaks displaying Warren-type line shapes.[58] This combination of absent peaks and line broadening indicates the formation of a layered phase similar to **hxl** UiO-67(Hf), but with turbostratic disorder in the *c*-direction. We propose the prefix **hns** ("hexagonal nanosheet") for this disordered layered phase.

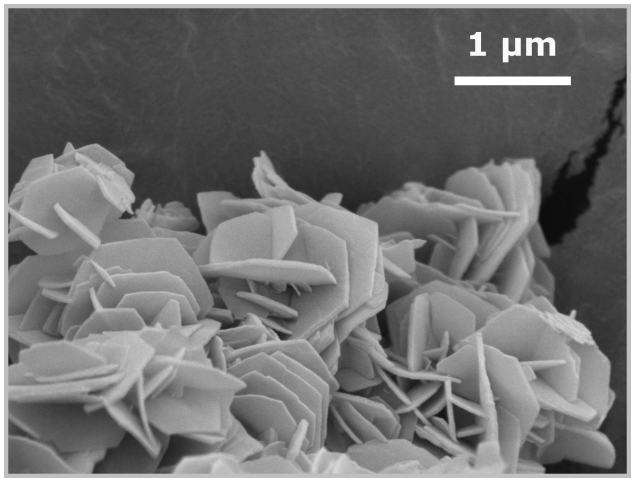

Fig. 3 SEM image of the **hns** phase of UiO-67(Hf), illustrating the hexagonal nano-sheet morphology.

Noting that dissociated water can compensate for missing-linker defects in UiO-66,[22,59] we then systematically investigated the effect of water in the synthesis of the **hcp** UiO-67(Hf) material. We now used anhydrous DMF solvent and added known volumes of water [Fig. 2(b)]. At low concentrations of water (i.e. where only a small amount of ambient water was present), **fcu** UiO-67 forms, along with a minor phase of **hcp**. The crystallinity and phase-purity of **hcp** UiO-67(Hf) is improved with small amounts of water used in the synthesis, as the added water suppresses the formation of any **fcu** impurity phase. At higher wa-

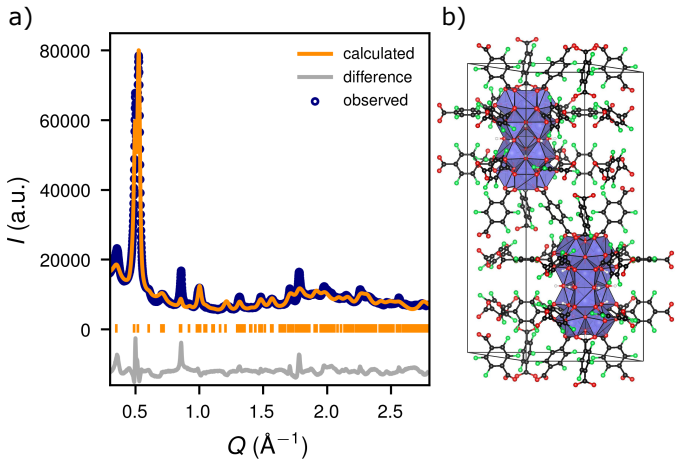

Fig. 4 a) Refinement of the PXRD pattern of **hcp** UiO-66(Hf) (F_4BDC) against b) the optimised model structure. The **hcp**-characteristic Hf_{12} double cluster is shown in the polyhedral representation. Discrepancies in low-Q peak intensities are likely to be due to the presence of guests in the pores.[9] Colour scheme of structure: Hf, blue; O, red; C, black; H, white; F, green.

ter concentrations, the **hns** phase forms, becoming phase-pure at 0.2 mL water (0.2:4 water:anhydrous DMF by volume) as shown by the complete loss of the **hcp** (102) peak. SEM imaging of this phase-pure **hns** UiO-67(Hf) sample [Fig. 3] reveals its hexagonal morphology. These materials, synthesised using water, are highly stable in ambient conditions; the washed **hcp** sample synthesised here using water is stable for up to 19 months, and the washed **hns** sample is still crystalline for up to 20 months [Figs. S1, S2], suggesting that thorough washing and activation of the sample tends to preserve the structural integrity of the framework by inhibiting the delamination we previously described (the **hcp** material produced by our previous synthesis was only stable for a few days).[9]

3.2 The Role of Water on UiO-66(Zr/Hf) (F_4BDC)

Observing the key role of water in the phase selection of UiO-67(Hf), we then examined other previously reported solvothermal syntheses of UiO materials where water was used as a solvent. The modulated hydrothermal methodology proposed by Ref. 43 provides a green and scalable approach to synthesising several frameworks isoreticular to **fcu** UiO-66(Zr). However, we noted that the material assigned as the cubic **fcu** UiO-66(Zr) (F_4BDC)[43,60] displays a characteristic splitting of the reflection indexed to the **fcu** (111) reflection into two peaks at 0.49 Å^{-1} and 0.52 Å^{-1}, and an additional reflection is present at 0.35 Å^{-1}. These features could be explained by this phase being the **hcp** rather than the **fcu** structure.

We therefore repeated the reported synthesis, producing both Zr and Hf analogues with experimental PXRD patterns consistent with those of Ref. 43. We were able to index the PXRD pattern of the Hf analogue using a hexagonal cell, and we carried out Pawley refinement[47] to obtain accurate unit cell and instrumental parameters [Fig. S3].

Using the experimental structure as a constraint, a model structure was derived from the known **hcp** UiO-67 structure.[9] This structure was then optimised using quantum chemical calculations. Density functional theory (DFT) calculations were performed both with and without the full crystal symmetry, to account for the tilting of the linkers. Optimisation with the full crystal symmetry constrains the linkers to be flat, which does not reflect the rotational disorder present in reality. Aside from the linker tilting, the model structures with and without the full symmetry are otherwise equivalent, giving no evidence of a symmetry-lowering distortion away from the hexagonal structure and suggesting that the overall symmetry of the UiO-66(Hf) (F_4BDC) structure is $P6_3/mmc$, like **hcp** UiO-67.

This triclinic optimised model, with linker tilting present, was then compared and validated against the experimental dataset, using the instrumental parameters obtained from the Pawley refinement [Fig. 4]. The background was modelled using a freely refining Chebyshev polynomial. Peak shapes were modelled using additional terms to account for anisotropic and size broadening and 2θ dependence. Due to the small crystallite size and resultant peak broadening, it was not possible to carry out Rietveld refinement.

While this water-rich synthesis of UiO-66 (F_4BDC) results in a **hcp** framework, it has been recently reported that an alternative route, with no added water and using THF as a solvent and hydrochloric acid as a modulator, produced the non-defective **fcu** phase.[44] Therefore, to understand the effect of the water content of the reaction on the phase of the resultant material, we systematically investigated the synthesis of UiO-66 (F_4BDC) with varying concentrations of water [Fig. 5]. In this series of syntheses, acetic acid was used as the modulator for consistency with the original reported hydrothermal synthesis.[43]

For UiO-66(Hf) (F_4BDC) synthesised hydrothermally with modulating acetic acid at both 120°C and 150°C, the phase which crystallises depends on the ratio of water to acid in the reaction mixture. These materials are very sensitive to the synthetic conditions, and the sample crystallinity is poor with low concentrations of modulating acetic acid. We found that with increasing concentrations of water the **hcp** material emerges, followed by a phase resembling **hns**. Thus both modulating acid and the presence of water are crucial to the formation of the **hcp** phase.

Furthermore, the **hcp** UiO-66(Hf) (F_4BDC) sample, like **hcp** UiO-67(Hf), transformed into a highly crystalline **hns** phase upon washing with DMF or methanol and activation [Fig. 5], showing that the creation of the defect-ordered **hcp** phase gives straightforward access to the layered-nanosheet material. SEM imaging [Fig. 6] shows the morphological differences between the **fcu**, **hcp** and **hns** phases; the **hcp** material shows a hexagonal intergrowth, with a characteristic 'desert rose' appearance, while the **hns** phase shows a delamination into sheets.

3.3 Synthesis of hcp UiO-66(Hf)

From the above two investigations, we have established that both modulating acid and water in the synthesis affect the phase of the material formed: increasing the concentration of acid and water simultaneously tends to promote the formation of the **hcp** phase

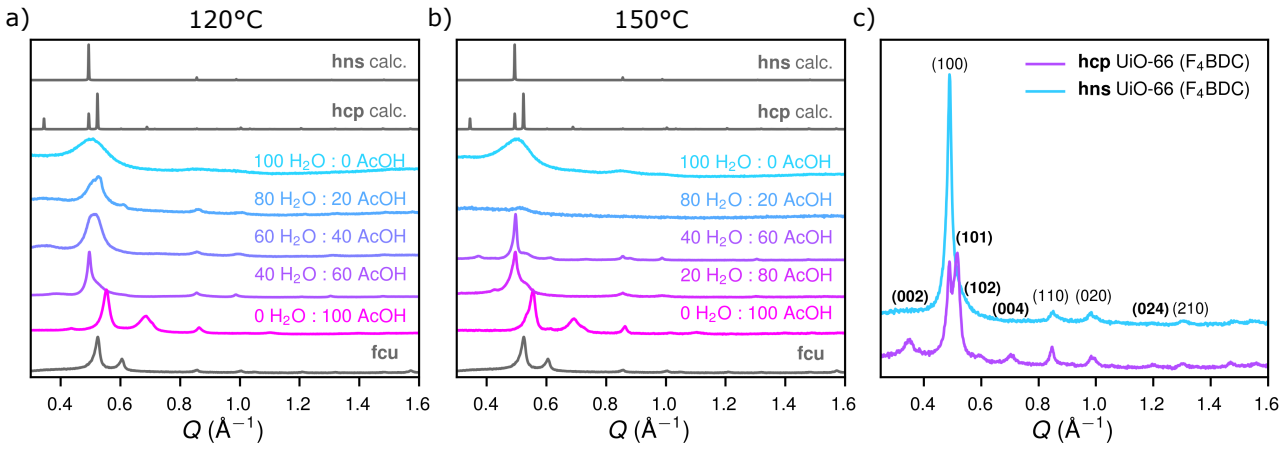

Fig. 5 a,b) PXRD patterns of UiO-66 (F_4BDC) synthesised with different water:acetic acid ratios at a) 120°C (temperature used in Ref. 43) and b) 150°C (the synthesis temperature for **hcp** UiO-67), compared with the predicted patterns for the **hcp** UiO-66(F_4BDC) structure. Synthesis conditions of 20% H_2O-80% AcOH (120°C) and 60% H_2O-40% AcOH (150°C) gave no product; c) comparison of the **hcp** (synthesised with 60:40 water:acetic acid at 120°C and **hns** (derived from the **hcp** by washing and activating) phases of UiO-66 (F_4BDC), showing the disappearance of *l*-dependent *hkl* peaks (labelled in bold) upon changing from **hcp** to **hns**.

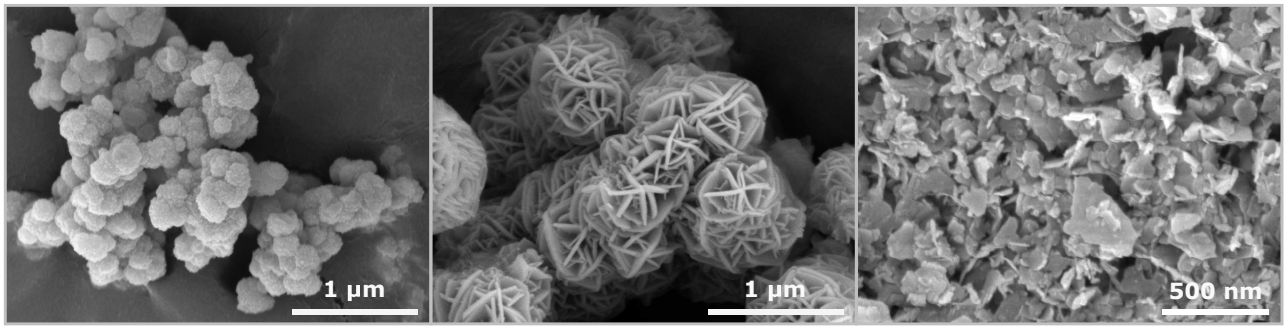

Fig. 6 SEM images of the different phases of UiO-66(Hf) (F_4BDC): left, **fcu** sample, synthesised based on the method of Ref. 44; centre, **hcp** sample, synthesised with 60:40 water:acetic acid at 120°C; right, **hns** sample, formed by delamination of the **hcp** material.

rather than the **fcu** or nano-**reo** structures. We then applied this understanding of the key role of water in synthesis, in combination with formic acid, to the pursuit of the **hcp** phase of UiO-66.

With high concentrations of water and formic acid we were able to synthesise phase-pure **hcp** UiO-66(Hf). At lower concentrations of either formic acid or water, the **fcu** (111) peak broadens into the region where **hcp** (100) and (101) peaks would be expected, but the individual **hcp** peaks are not seen, indicative of a low concentration of **hcp** (**fcu** remaining the major component); phase-pure **hcp** UiO-66(Hf) only forms once volumes of 0.4 mL water and 1.5 mL formic acid are used [Fig. 7(a-d)]. The PXRD pattern of this material is consistent with that recently reported by Ref. 46 for the **hcp** UiO-66(Zr) material.

To confirm the assignment of this phase as **hcp**, a model structure of **hcp** UiO-66(Hf) was created based on our optimised structure for **hcp** UiO-66(Hf) (F_4BDC). Using the same approach as used to analyse the PXRD pattern of **hcp** UiO-66(Hf) (F_4BDC), the PXRD pattern of **hcp** UiO-66(Hf) was indexed, and accurate unit cell and instrumental parameters obtained from Pawley refinement [Fig. S4]. These parameters were then used in a comparison of the experimental **hcp** dataset against the model structure, which gave a good fit [Fig. 8(a,b)]. The background and peak shapes were modelled using the same approach as for the **hcp** UiO-66(Hf) (F_4BDC) structure, with an additional term to account for preferred orientation along [001]. Again, due to the small crystallite size, it was not possible to carry out Rietveld refinement.

Further increasing the volumes of water and formic acid in the reaction mixture to a maximum of 3.5 mL and 3.0 mL respectively produced neither the hafnium formate phase previously reported for both UiO-66(Hf) and UiO-67(Hf), nor the phase-pure delaminated **hns** phase seen in the investigation of **hcp** UiO-67 [Figs. S5-S7]. Thus again water, alongside modulating acid, is important in obtaining the **hcp** phase of UiO-66, both by promoting the formation of the **hcp** structure over the **fcu**, and by suppressing the hafnium formate phase. The washed and activated **hcp** UiO-66(Hf) material synthesised in this manner is stable in ambient conditions, with little change observed in the PXRD after nine months (at the time of writing) [Fig. S8]. We note that it is markedly easier to delaminate **hcp** UiO-66 (F_4BDC) than **hcp** UiO-66 (BDC), and ascribe this to the increased lability of the more acidic F_4BDC linker.

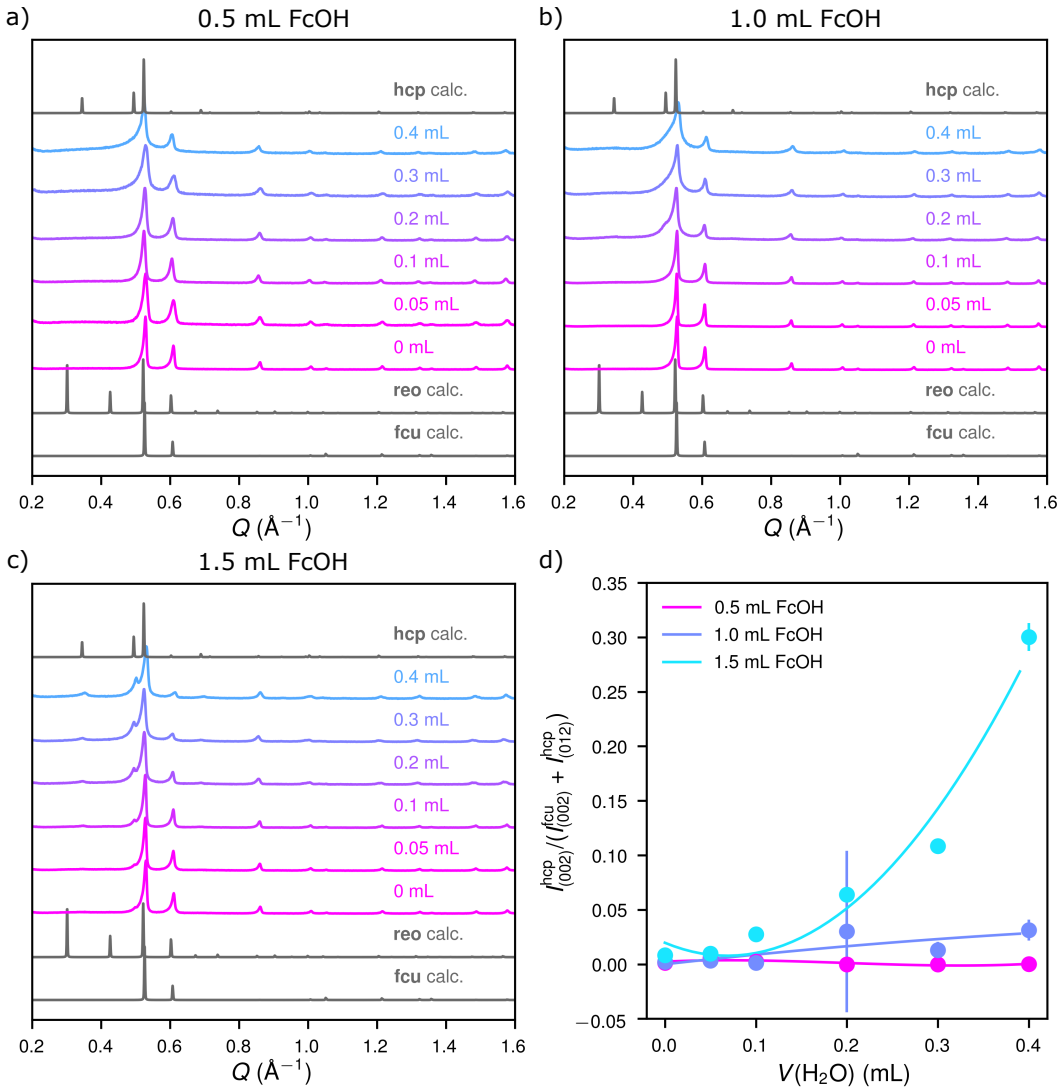

Fig. 7 a-c) PXRD patterns of UiO-66 synthesised with varying water concentrations and a) 0.5 mL FcOH; b) 1.0 mL FcOH; c) 1.5 mL FcOH. d) Plot of the intensity ratio of **hcp** vs **fcu** peaks, showing the emergence of the **hcp** UiO-66 phase only at higher concentrations of both formic acid and water. PXRD patterns are compared with the predicted patterns for the **fcu**,[6] **reo**[19] and **hcp** UiO-66 structures.

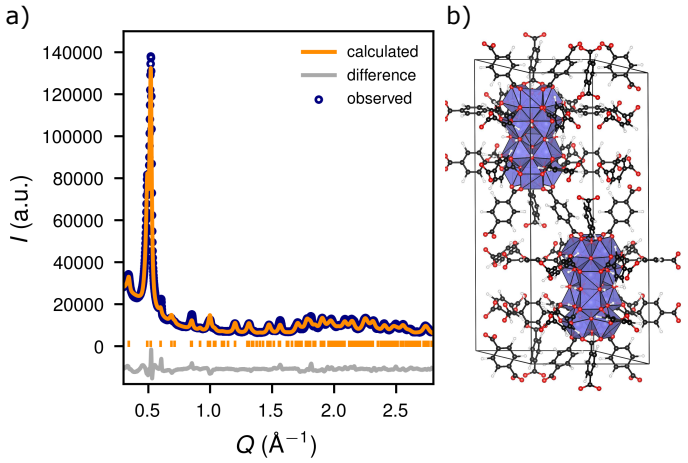

Fig. 8 a) Refinement of the PXRD pattern of **hcp** UiO-66 against b) the proposed structure. Discrepancies in low-Q peak intensities are likely to be due to the presence of guests in the pores.[9] Colour scheme of structure: Hf, blue; O, red; C, black; H, white.

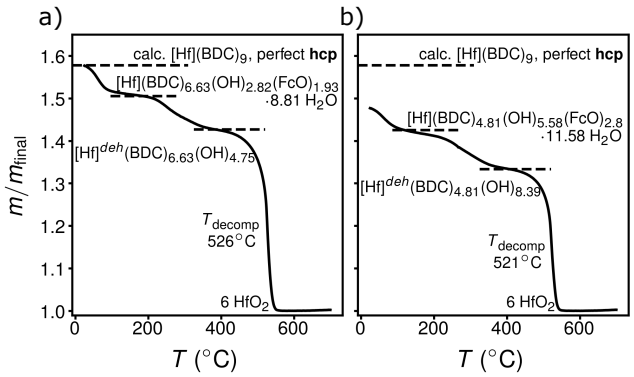

Fig. 9 TGA curves for **hcp** UiO-66 synthesised with a) 1.5 mL formic acid and 0.4 mL water; b) 1.5 mL formic acid and 1.5 mL water. [Hf] represents the $(Hf_6O_4(OH)_4)_2(OH)_6$ cluster, and [Hf]^{deh} represents the dehydroxylated $(Hf_6O_6)_2(OH)_6$ cluster; the calculated mass fraction for a perfect, non-defective **hcp** sample is shown for comparison.

3.4 Investigation of Defect Concentrations in hcp UiO-66(Hf) Phases via TGA and ^{1}H NMR Studies

While the formation of **hcp** UiO-66(Hf) occurs at higher concentrations of both formic acid and water (0.4 mL water and 1.5 mL formic acid in 4 mL anhydrous DMF) than for **hcp** UiO-67(Hf) (0.05 mL water and 1 mL formic acid), missing-linker defects are formed more easily in **fcu** UiO-66 than in UiO-67[22,61,62] and it is likely that a higher concentration of defects can be stabilised in **fcu** UiO-66(Hf) compared to **fcu** UiO-67(Hf) before the defect-ordered **hcp** phase forms.[63]

It is well known that modulated synthesis of **fcu** UiO-66, often introduces missing-linker defects, whereas these are rare in **fcu** UiO-67. These missing-linker defects are compensated by modulating acid, water, or hydroxide.[9,21,22] While the recently-reported **hcp** UiO-66(Zr) was briefly noted to contain missing-linker defects,[46] we have investigated the presence of defect-compensating molecules in **hcp** UiO-66(Hf), to establish whether water and formic acid in the synthesis not only determine the phase, as we have demonstrated, but also control the concentration of missing-linker defects in the **hcp** phase, just as in **fcu** UiO-66.[64]

We used thermogravimetric analysis (TGA) to calculate the amount of missing-linker defects. The TGA analysis of UiO-66 family frameworks shows three distinct steps, corresponding to different stages of decomposition. The first significant mass losses (below 150°C) are due to the loss of solvent molecules and hydrogen-bonded water.[59] The mass losses between 250 and 300°C correspond to the dehydroxylation of the $Hf_6O_4(OH)_4$ cluster to Hf_6O_6,[8,65] as well as loss of missing-linker-compensating formate or water molecules.[6,14,59] The final and largest mass loss, used to calculate the linker-cluster stoichiometry, corresponds to the decomposition of the remaining framework and the formation of HfO_2.[65,66] TGA analysis of **hcp** UiO-66 samples [Fig. S11] likewise displays mass losses at similar temperatures; however, in the 'dehydroxylation' step, we assumed that the Hf_{12} double cluster does not dissociate via loss of the six μ_2-OH, instead losing formate (FcO) and hydrogen-bonded water as with **fcu** UiO-66 to give a $(Hf_6O_6)_2(OH)_6$ dehydroxylated double cluster. A detailed discussion of the mass losses in the TGA can be found in the ESI.

Of the UiO-66 samples synthesised with 1.5 mL formic acid, those with >0.4 mL water are phase-pure **hcp** UiO-66 by PXRD. However, the ratios of initial to final masses for these samples are lower than for perfect **hcp**, indicating the presence of defects, and also show a correlation between the lowering of the framework mass and the concentration of water in the synthesis [Fig. S11]. Samples with 0–0.3 mL water in the reaction mixture are mixed-phase; their mass ratios compared to HfO_2 are lower than for perfect **fcu**, as expected for a **fcu**/**hcp** mixture since **hcp** UiO-66 has a lower metal:linker ratio than **fcu**. However, without the PXRD data, these TGA curves could be erroneously modelled as extremely defective **fcu**. This demonstrates the need for care when using TGA data to calculate the defect concentration in UiO samples: if a sample is mixed phase, or the wrong model structure is used, there will be large systematic errors in the estimated defectivity.

The presence of formate (FcO) in the above activated phase-pure **hcp** UiO-66 frameworks was confirmed by solution ^{1}H NMR [Figs. S12,S13]; further deviations from the expected mass fraction indicate the presence of water or hydroxide as additional capping molecules. Where the formula of defect-free **hcp** UiO-66(Hf) is $[Hf_6O_4(OH)_4]_2(OH)_6(BDC)_9$, the formulae of defective samples containing defect-compensating formate, water and hydroxide molecules can be written as $[(Hf_6O_4(OH)_4)_2(OH)_6](BDC)_x(OH)_y(FcO)_z{\cdot}n\,H_2O$. The **hcp** UiO-66 sample synthesised with 0.4 mL water and 1.5 mL formic acid is found to have $x = 6.63(11)$, $y = 2.82(22)$, $z = 1.93(4)$, $n = 8.81(22)$, i.e. with 26(1) % of terephthalate (BDC) linkers replaced. For the sample synthesised with 1.5 mL water and 1.5 mL formic acid, this gives $x = 4.81(11)$, $y = 5.58(22)$, $z = 2.80(7)$, $n = 11.58(22)$, i.e. with 47(1) % of BDC linkers replaced [Fig. 9, Table S2]. Therefore the **hcp** material can incorporate missing-linker defects to a high level, compensated by both formate and water/hydroxide, as in **fcu** UiO-66. Water in the synthesis also allows control over the phase purity of the sample.

Hence not only the phase but also the defectivity of the sample can be tuned by adjusting the water concentration in the synthesis.

3.5 Adsorption Isotherm Measurements of hcp UiO-66(Hf)

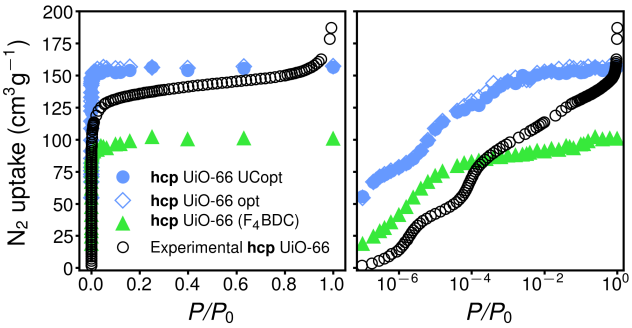

Fig. 10 Simulated and experimental N_2 isotherms for **hcp** UiO-66 (right: semi-logarithmic scale). The simulated N_2 adsorption isotherm for UiO-66 (F_4BDC) is plotted for comparison.

The change in the structure due to the cluster condensation from **fcu** to **hcp** affects the surface area and size of the pores in the sample, as demonstrated by its sorption behaviour [Fig. 10]. The new phase **hcp** UiO-66 (Hf) has a Brunauer-Emmett-Teller (BET) area (N_2) of 422 m^2g^{-1} (when synthesised with 0.4 mL water), which is lower than the 655–940 m^2g^{-1} of the **fcu** UiO-66 (Hf) phase.[19,67–69] This is expected due to the greater density of the double-cluster material as opposed to the single cluster phase, and is also displayed in **hcp** compared to **fcu** UiO-67 and, more generally, in the cluster condensation of oxide materials.[9,70]

The simulated N_2 adsorption isotherms [Fig. 10], using grand canonical Monte Carlo (GCMG) calculations, based on the model **hcp** UiO-66 crystal structure, agree well with the experimentally-observed isotherms at saturation pressures.[53,69] At lower pressure, they show a typical overprediction of the host-guest interaction.[71] The simulations were performed using two **hcp** UiO-66 structures generated from the model **hcp** structure of UiO-66 (F_4BDC). The first structure (**hcp** UiO-66 (opt)) corresponds to the geometrically optimized material after exchanging all F atoms to H while keeping the unit cell parameters fixed. The second structure (**hcp** UiO-66 (UCopt)) was generated by optimizing the geometry while relaxing the unit cell parameters. The simulations for both of these structures, carried out at 77 K, almost overlap, suggesting that the proposed **hcp** UiO-66 structure is very close to the known **hcp** UiO-66 (F_4BDC) structure and does not show any flexibility. For comparison, the BET area of 370–380 m^2g^{-1} calculated for **hcp** UiO-66 (F_4BDC) from these simulations agrees with the published BET value of 328 m^2g^{-1}.[43]

Usually for microporous powder samples, a Type I isotherm is seen, corresponding to the filling of the narrow pores with large affinity to the guest (N_2) molecules; this is seen in the simulated isotherm, performed on a perfect model crystal without any defects.[72] In our case, however, the experimental isotherm of **hcp** UiO-66 is of Type II, displaying a small positive slope in the range 0.0001–0.9 P/P_0, followed by a suddenly increased uptake at high P/P_0,[1,72,73] and therefore indicating the presence in the sample of mesoporosity.[11,12,22,37] In this regard, missing-linker defects in **fcu** UiO-66 are known to create mesopores;[1] in UiO-66 samples with missing-linker defects and known mesoporosity, pore volumes of up to 1.0 cm^3g^{-1}, corresponding to pore apertures of 11.5 Å, and diameters even of 1–5.5 nm have been observed.[1,19,33,74] This is in comparison to purely microporous UiO-66, which yields pore volumes of 0.426 cm^3g^{-1}, with 6 Å apertures and 30 Å diameter.[8,10,75] Here, calculations from the isotherms of **hcp** UiO-66 give a Horvath-Kawazoe pore width of 7.13 Å and average pore diameter of 68.7 Å, which support the existence of mesopores in the **hcp** sample.[76–80]

4 Conclusions

In this work, we have demonstrated that water plays a key role in the synthesis of defect phases of UiO family MOFs. We have shown that both water and formic acid are instrumental in allowing control over the phase formed, causing the condensation of the metal clusters into the Hf_{12} double clusters characteristic of the **hcp** phase [Fig. 11]. Starting from the first known example of the **hcp** phase, **hcp** UiO-67, we applied the discovery of the critical role of water in phase-selection to other members of the UiO family and used this understanding to synthesise the **hcp** phase of the canonical UiO-66, using conventional solvents rather than complex or expensive systems. We have also established that water and hydroxide can introduce missing-linker defects into this framework by replacing the bidentate dicarboxylate linkers, and therefore that by controlling the concentration of water in the synthesis the number of such defects in the sample can be tuned. Characterisation of the **hcp** UiO-66(Hf) material has shown that it can sustain missing-linker defects to high concentrations compensated by the introduction of formate, water and hydroxide groups, creating mesopores as shown by pore size measurements. Moreover, the introduction of directionally-correlated missing-linker defects through this defect-engineering process has allowed us to directly synthesise two-dimensional UiO MOF nanosheets with hexagonal topology, **hns** UiO-66 (F_4BDC) and **hns** UiO-67 [Fig. 11].

While the key role of water, as well as formic acid, in the creation of missing-linker defects and hence these new defect-engineered phases is evident, and a degree of control over the phase formation and purity has been obtained, work is now in progress to investigate the mechanism through which this occurs. Moreover, the inclusion at different locations of new water and hydroxide groups may create new sites of Brønsted acidity[1] and affect the sorption behaviour, hydrophilicity and catalytic behaviour of the framework. Finally, the creation of novel stable Zr/Hf MOF-based nanosheets in this way represents a potential strategy for synthesising MOF membranes.

Conflicts of interest

There are no conflicts to declare.

Acknowledgements

The authors thank Dr Heather Greer for assistance running SEM and Dr David Halat for assistance with TGA. F.C.N.F. was sup-

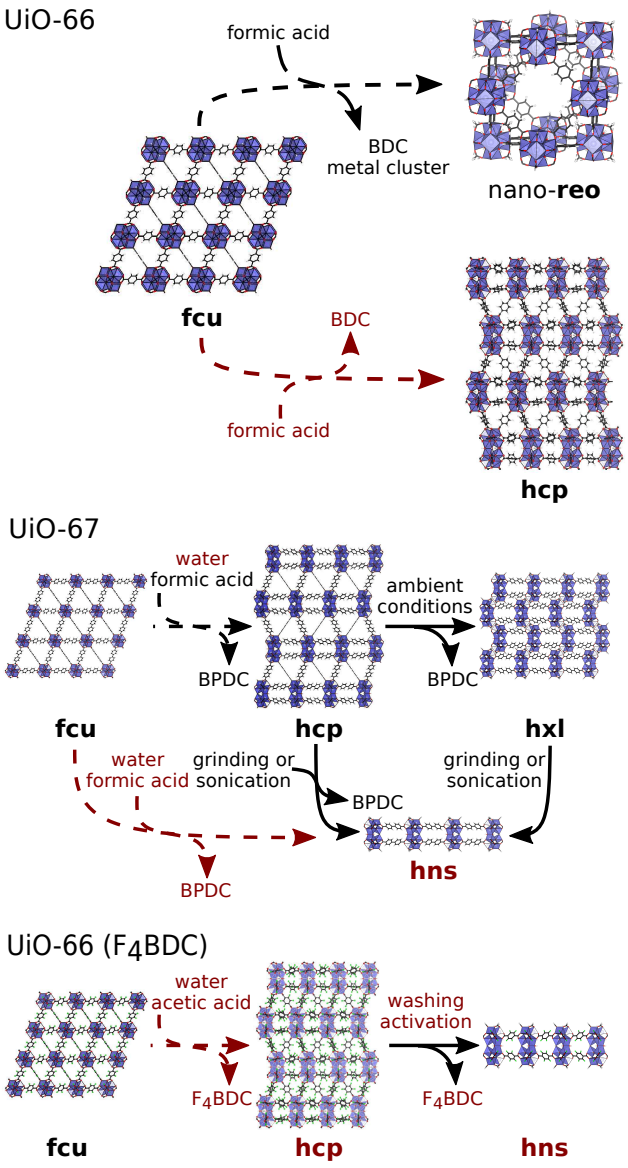

Fig. 11 Summary of the reported and new phases of UiO-66 (top), UiO-67 (centre) and UiO-66 (F_4BDC) (bottom). Dashed arrows show the differences in the synthesis conditions used to prepare different phases; solid arrows show postsynthetic treatments. Text in black indicates phases or syntheses already known prior to this report; text in red indicates phases or syntheses discovered or assigned in this report. Crystal files of previously-reported phases from Refs. 6,9,19

ported by the Engineering and Physical Sciences Research Council (U.K.). M.J.C. was supported by Sidney Sussex College, Cambridge and by the European Research Council (279705); C.P.G. was supported by the Engineering and Physical Sciences Research Council (U.K.) under the Supergen Consortium and Grant (EP/N001583/1). D.F.-J. thanks the Royal Society for funding through a University Research Fellowship.

Notes and references

1 H. Wu, Y. S. Chua, V. Krungleviciute, M. Tyagi, P. Chen, T. Yildirim and W. Zhou, *J. Am. Chem. Soc.*, 2013, **135**, 10525–10532.

2 W. Xia, A. Mahmood, R. Zou and Q. Xu, *Energy Environ. Sci.*, 2015, **8**, 1837–1866.

3 F.-S. Ke, Y.-S. Wu and H. Deng, *J. Solid State Chem.*, 2015, **223**, 109–121.

4 F. Su, S. Zhang, H. Ji, H. Zhao, J.-Y. Tian, C.-S. Liu, Z. Zhang, S. Fang, X. Zhu and M. Du, *ACS Sensors*, 2017, **2**, 998–1005.

5 H. Sun, B. Tang and P. Wu, *ACS Appl. Mater. Interfaces*, 2017, **9**, 26077–26087.

6 M. J. Cliffe, J. A. Hill, C. A. Murray, F.-X. Coudert and A. L. Goodwin, *Phys. Chem. Chem. Phys.*, 2015, **17**, 11586–11592.

7 M. Bosch, S. Yuan and H.-C. Zhou, in *The Chemistry of Metal-Organic Frameworks: Synthesis, Characterisation, and Applications*, ed. S. Kaskel, Wiley-VCH Verlag GmbH & Co., 2016, ch. 6, pp. 137–170.

8 J. H. Cavka, S. Jakobsen, U. Olsbye, N. Guillou, C. Lamberti, S. Bordiga and K. P. Lillerud, *J. Am. Chem. Soc.*, 2008, **130**, 13850–13851.

9 M. J. Cliffe, E. Castillo-Martínez, Y. Wu, J. Lee, A. C. Forse, F. C. Firth, P. Z. Moghadam, D. Fairen-Jimenez, M. W. Gaultois, J. A. Hill, O. V. Magdysyuk, B. Slater, A. L. Goodwin and C. P. Grey, *J. Am. Chem. Soc.*, 2017, **139**, 5397–5404.

10 C. L. Luu, T. T. V. Nguyen, T. Nguyen and T. C. Hoang, *Adv. Nat. Sci. Nanosci. Nanotechnol.*, 2015, **6**, 025004.

11 W. Liang, C. J. Coghlan, F. Ragon, M. Rubio-Martinez, D. M. D'Alessandro and R. Babarao, *Dalton Trans.*, 2016, **45**, 4496–4500.

12 P. Xydias, I. Spanopoulos, E. Klontzas, G. E. Froudakis and P. N. Trikalitis, *Inorg. Chem.*, 2014, **53**, 679–681.

13 F. Vermoortele, B. Bueken, G. Le Bars, B. Van De Voorde, M. Vandichel, K. Houthoofd, A. Vimont, M. Daturi, M. Waroquier, V. Van Speybroeck, C. Kirschhock and D. E. De Vos, *J. Am. Chem. Soc.*, 2013, **135**, 11465–11468.

14 G. C. Shearer, S. Chavan, S. Bordiga, S. Svelle, U. Olsbye and K. P. Lillerud, *Chem. Mater.*, 2016, **28**, 3749–3761.

15 Z. Fang, B. Bueken, D. E. De Vos and R. A. Fischer, *Angew. Chemie - Int. Ed.*, 2015, **54**, 7234–7254.

16 M. Shoaee, M. Anderson and M. Attfield, *Angew. Chemie - Int. Ed.*, 2008, **47**, 8525–8528.

17 G. C. Shearer, J. G. Vitillo, S. Bordiga, S. Svelle, U. Olsbye and K. P. Lillerud, *Chem. Mater.*, 2016, **28**, 7190–7193.

18 S. Dissegna, K. Epp, W. R. Heinz, G. Kieslich and R. A. Fischer, *Adv. Mater.*, 2018, **30**, 1704501.

19 M. J. Cliffe, W. Wan, X. Zou, P. A. Chater, A. K. Kleppe, M. G. Tucker, H. Wilhelm, N. P. Funnell, F.-X. Coudert and A. L. Goodwin, *Nat. Commun.*, 2014, **5**, 4176.

20 G. Mouchaham, L. Cooper, N. Guillou, C. Martineau, E. Elkaïm, S. Bourrelly, P. L. Llewellyn, C. Allain, G. Clavier, C. Serre and T. Devic, *Angew. Chemie - Int. Ed.*, 2015, **54**, 13297–13301.

21 S. Ayala Jr., Z. Zhang and S. M. Cohen, *Chem. Commun.*, 2017, **53**, 3058–3061.

22 O. V. Gutov, M. G. Hevia, E. C. Escudero-Adán and A. Shafir, *Inorg. Chem.*, 2015, **54**, 8396–8400.

23 A. S. Solovkin and Z. N. Tsvetkova, *Russ. Chem. Rev.*, 1962,

31, 655–659.
24 B. A. J. Lister and L. A. McDonald, *J. Chem. Soc.*, 1952, 4315–4330.
25 B. I. Intorre and A. E. Martell, *J. Am. Chem. Soc.*, 1960, **82**, 358–364.
26 V. V. Kanazhevskii, B. N. Novgorodov, V. P. Shmachkova, N. S. Kotsarenko, V. V. Kriventsov and D. I. Kochubey, *Mendeleev Commun.*, 2001, **11**, 211–212.
27 Y. Saku, Y. Sakai, A. Shinohara, K. Hayashi, S. Yoshida, C. N. Kato, K. Yoza and K. Nomiya, *Dalton Trans.*, 2009, **3**, 805–813.
28 T. Kobayashi, T. Sasaki, I. Takagi and H. Moriyama, *J. Nucl. Sci. Technol.*, 2009, **46**, 142–148.
29 D. N. Bunck and W. R. Dichtel, *Chem. - Eur. J.*, 2013, **19**, 818–827.
30 G. Wißmann, A. Schaate, S. Lilienthal, I. Bremer, A. M. Schneider and P. Behrens, *Microporous Mesoporous Mater.*, 2012, **152**, 64–70.
31 A. Schaate, P. Roy, A. Godt, J. Lippke, F. Waltz, M. Wiebcke and P. Behrens, *Chem. - Eur. J.*, 2011, **17**, 6643–51.
32 M. J. Katz, Z. J. Brown, Y. J. Colón, P. W. Siu, K. a. Scheidt, R. Q. Snurr, J. T. Hupp and O. K. Farha, *Chem. Commun.*, 2013, **49**, 9449–51.
33 G. Cai and H.-L. Jiang, *Angew. Chemie - Int. Ed.*, 2017, **56**, 563–567.
34 W. Liang, R. Babarao, M. J. Murphy and D. M. D'Alessandro, *Dalton Trans.*, 2015, **44**, 1516–1519.
35 D. J. Ashworth and J. A. Foster, *J. Mater. Chem. A*, 2018, **6**, 16292–16307.
36 Y. Zhao, Z. Song, X. Li, Q. Sun, N. Cheng, S. Lawes and X. Sun, *Energy Storage Mater.*, 2016, **2**, 35–62.
37 P. Ghosh, Y. J. Colón and R. Q. Snurr, *Chem. Commun.*, 2014, **50**, 11329–11331.
38 G. C. Shearer, S. Chavan, J. Ethiraj, J. G. Vitillo, S. Svelle, U. Olsbye, C. Lamberti, S. Bordiga and K. P. Lillerud, *Chem. Mater.*, 2014, **26**, 4068–4071.
39 D. H. Devia and A. G. Sykes, *Inorg. Chem.*, 1981, **20**, 910–913.
40 C. Ekberg, G. Källvenius, Y. Albinsson and P. L. Brown, *J. Solution Chem.*, 2004, **33**, 47–79.
41 R. D'Amato, A. Donnadio, M. Carta, C. Sangregorio, R. Vivani, D. Tiana, M. Taddei and F. Costantino, *ACS Sustain. Chem. Eng.*, 2019, **7**, 394–402.
42 S. Waitschat, H. Reinsch and N. Stock, *Chem. Commun.*, 2016, **52**, 12698–12701.
43 Z. Hu, A. Nalaparaju, Y. Peng, J. Jiang and D. Zhao, *Inorg. Chem.*, 2016, **55**, 1134–1141.
44 P. Ji, T. Drake, A. Murakami, P. Oliveres, J. H. Skone and W. Lin, *J. Am. Chem. Soc.*, 2018, **140**, 10553–10561.
45 P. Ji, K. Manna, Z. Lin, X. Feng, A. Urban, Y. Song and W. Lin, *J. Am. Chem. Soc.*, 2017, **139**, 7004–7011.
46 M. Ermer, J. Mehler, M. Kriesten, Y. Avadhut, P. S. Schulz and M. Hartmann, *Dalt. Trans.*, 2018, **47**, 14426–14430.
47 G. S. Pawley, *J. Appl. Crystallogr.*, 1981, **14**, 357–361.
48 H. M. Rietveld, *J. Appl. Crystallogr.*, 1969, **2**, 65–71.
49 A. A. Coelho, *J. Appl. Crystallogr.*, 2018, **51**, 210–218.
50 C. F. Macrae, I. J. Bruno, J. A. Chisholm, P. R. Edgington, P. McCabe, E. Pidcock, L. Rodriguez-Monge, R. Taylor, J. Van De Streek and P. A. Wood, *J. Appl. Crystallogr.*, 2008, **41**, 466–470.
51 K. Momma and F. Izumi, *J. Appl. Crystallogr.*, 2011, **44**, 1272–1276.
52 G. Nickerl, M. Leistner, S. Helten, V. Bon, I. Senkovska and S. Kaskel, *Inorg. Chem. Front.*, 2014, **1**, 325–330.
53 D. Dubbeldam, S. Calero, D. E. Ellis and R. Q. Snurr, *Mol. Simul.*, 2015, **42**, 81–101.
54 J. J. Potoff and J. I. Siepmann, *AIChE J.*, 2001, **47**, 1676–1682.
55 A. K. Rappé, C. J. Casewit, K. S. Colwell, W. A. Goddard III and W. M. Skiff, *J. Am. Chem. Soc.*, 1992, **114**, 10024–10035.
56 H. Lorentz, *Ann. Phys.*, 1881, **248**, 127–136.
57 D. Berthelot, *C. R. Hebd. Séances Acad. Sci.*, 1898, **126**, 1703–1855.
58 B. E. Warren, *Phys. Rev.*, 1941, **59**, 693–698.
59 S. Ling and B. Slater, *Chem. Sci.*, 2016, **7**, 4706–4712.
60 Z. Hu, Y. Peng, Z. Kang, Y. Qian and D. Zhao, *Inorg. Chem.*, 2015, **54**, 4862–4868.
61 R. C. Klet, Y. Liu, T. C. Wang, J. T. Hupp and O. K. Farha, *J. Mater. Chem. A*, 2016, **4**, 1479–1485.
62 S. Øien, D. Wragg, H. Reinsch, S. Svelle, S. Bordiga, C. Lamberti and K. P. Lillerud, *Cryst. Growth Des.*, 2014, **14**, 5370–5372.
63 J. B. DeCoste, G. W. Peterson, H. Jasuja, T. G. Glover, Y.-g. Huang and K. S. Walton, *J. Mater. Chem. A*, 2013, **1**, 5642–5650.
64 M. R. Momeni and C. J. Cramer, *Chem. Mater.*, 2018, **30**, 4432–4439.
65 G. C. Shearer, S. Forselv, S. Chavan, S. Bordiga, K. Mathisen, M. Bjørgen, S. Svelle and K. P. Lillerud, *Top. Catal.*, 2013, **56**, 770–782.
66 L. Valenzano, B. Civalleri, S. Chavan, S. Bordiga, M. H. Nilsen, S. Jakobsen, K. P. Lillerud and C. Lamberti, *Chem. Mater.*, 2011, **23**, 1700–1718.
67 S. Jakobsen, D. Gianolio, D. S. Wragg, M. H. Nilsen, H. Emerich, S. Bordiga, C. Lamberti, U. Olsbye, M. Tilset and K. P. Lillerud, *Phys. Rev. B*, 2012, **86**, 125429.
68 U. Ravon, M. Savonnet, S. Aguado, M. E. Domine, E. Janneau and D. Farrusseng, *Microporous Mesoporous Mater.*, 2010, **129**, 319–329.
69 S. Brunauer, P. H. Emmett and E. Teller, *J. Am. Chem. Soc.*, 1938, **60**, 309–319.
70 S. Andersson, A. Sundholm and A. Magnéli, *Acta Chem. Scand.*, 1959, **13**, 989–997.
71 D. Fairen-Jimenez, R. Galvelis, A. Torrisi, A. D. Gellan, M. T. Wharmby, P. A. Wright, C. Mellot-Draznieks and T. Düren, *Dalt. Trans.*, 2012, **41**, 10752.
72 S. Lowell and J. E. Shields, in *Powder Surface Area and Porosity*, Springer, Dordrecht, 1984, pp. 11–13.

73 P. Schneider, *Appl. Catal. A, Gen.*, 1995, **129**, 157–165.
74 B. Li, X. Zhu, K. Hu, Y. Li, J. Feng, J. Shi and J. Gu, *J. Hazard. Mater.*, 2016, **302**, 57–64.
75 G. W. Peterson, S.-Y. Moon, G. W. Wagner, M. G. Hall, J. B. Decoste, J. T. Hupp and O. K. Farha, *Inorg. Chem.*, 2015, **54**, 9684–9686.
76 G. Horvath and K. Kawazoe, *J. Chem. Eng. Japan*, 1983, **16**, 470–475.
77 R. J. Dombrowski, C. M. Lastoskie and D. R. Hyduke, *Colloids Surf., A*, 2001, **187-188**, 23–39.
78 E. P. Barrett, L. G. Joyner and P. P. Halenda, *J. Am. Chem. Soc.*, 1951, **73**, 373–380.
79 L. S. Cheng and R. T. Yang, *Chem. Eng. Sci.*, 1994, **49**, 2599–2609.
80 A. Saito and H. C. Foley, *AIChE J.*, 1991, **37**, 429–436.